

## State-dependent decoupling of sensory and motor circuits underlies behavioral flexibility in *Drosophila*

Jan M. Ache<sup>1</sup>, Shigehiro Namiki<sup>1,2</sup>, Allen Lee<sup>1,3</sup>, Kristin Branson<sup>1</sup>, Gwyneth M. Card<sup>1,\*</sup>

<sup>1</sup>Howard Hughes Medical Institute, Janelia Research Campus, Ashburn, Virginia, USA

<sup>2</sup>Research Center for Advanced Science and Technology, The University of Tokyo, Tokyo, Japan

<sup>3</sup>Leap Scientific LLC, Hooksett, New Hampshire

### Abstract

An approaching predator and self-motion towards an object can generate similar looming patterns on the retina, but these situations demand different rapid responses. How central circuits flexibly process visual cues to activate appropriate, fast motor pathways remains unclear. Here, we identify two descending neuron (DN) types that control landing and contribute to visuomotor flexibility in *Drosophila*. For each, silencing impairs visually-evoked landing, activation drives landing, and spike rate determines leg extension amplitude. Critically, visual responses of both DNs are severely attenuated during non-flight periods, effectively decoupling visual stimuli from the landing motor pathway when landing is inappropriate. The flight-dependence mechanism differs between DN types. Octopamine exposure mimics flight effects in one, whereas the other likely receives neuronal feedback from flight motor circuits. Thus, this sensorimotor flexibility arises from distinct mechanisms for gating action-specific descending pathways, such that sensory and motor networks are coupled or decoupled according to the behavioral state.

### Introduction

Looming patterns are salient natural cues that occur on an observer's retina when they approach an object, or when an object, such as a predator, approaches them. In *Drosophila*, a direct feedforward pathway linking looming-sensitive visual neurons to escape behavior has been resolved at the neuronal level. On either side of the brain, two visual projection neuron

---

Users may view, print, copy, and download text and data-mine the content in such documents, for the purposes of academic research, subject always to the full Conditions of use: [http://www.nature.com/authors/editorial\\_policies/license.html#terms](http://www.nature.com/authors/editorial_policies/license.html#terms)

\*Corresponding author: [cardg@janelia.hhmi.org](mailto:cardg@janelia.hhmi.org).

#### Author contributions

J.M.A. conceived the project, designed experiments, performed patch-clamp recordings, performed behavioral and optogenetic activation experiments, wrote analysis code, analyzed the data, generated the figures, and wrote the manuscript. S.N. designed experiments, performed and analyzed behavioral optogenetic activation experiments, generated split-GAL4 driver lines, and contributed anatomy figures. A.L. and K.B. developed tracking software. G.M.C. conceived the project, designed experiments, wrote the manuscript, and provided supervision.

#### Competing interests

The authors declare no competing interests.

#### Data availability

The data and analysis code that support the findings of this study are available from the corresponding author upon reasonable request. The leg tracking software was deposited to <https://github.com/kristinbranson/APT>.

types from the optic lobes<sup>1,2</sup> act as looming-feature detectors and synapse directly onto the Giant Fiber descending neuron (DN), which fires a single action potential to activate motor neurons in the ventral nerve cord (VNC)<sup>3-5</sup>. This circuit mediates a rapid, short-duration escape takeoff in response to looming predators<sup>6</sup>. However, flies also experience looming stimuli in other behavioral contexts, such as when flying towards an object (Fig. 1a) or walking towards a conspecific. In these cases, the fly does not takeoff, but rather lands<sup>7,8</sup> or lets the other fly pass<sup>9</sup>, respectively. Similar cues can also lead to context-dependent attractive or aversive behavioral responses in vertebrates<sup>10</sup>.

Given the ambiguity of looming cues, it is unclear how the central nervous system produces appropriate, distinct behavioral responses, depending on context or behavioral state. In some cases, looming sensorimotor pathways for different behaviors are tuned to distinct stimulus parameters. For example, in flying flies, frontal looming stimuli elicit a landing response, whereas lateral looming stimuli drive an evasive saccade<sup>7,11</sup>, and in mice, the visual contrast of a looming stimulus influences whether it triggers freezing or an escape response<sup>12</sup>. However, in cases where different behaviors can be triggered by stimuli with identical parameters, action selection must be mediated by other mechanisms. Here, we show that the same looming stimulus that triggers escape also evokes landing responses in *Drosophila* and identify two DN types that control landing. We then leverage this discovery to unravel the mechanisms by which neuronal activity is flexibly channeled from sensory circuits in the brain to motor networks in the VNC.

## Results

To test whether escape behavior (in perching flies) and landing behavior (in flying flies) can be elicited by stimuli with identical parameters, we repeatedly presented a frontal looming stimulus to tethered flies surrounded by an LED display (Fig. 1b). Each trial began with a tethered fly either perched on a ‘diving board’ (Fig. 1b, black lines) or (gray lines). In perching flies, looming elicited typical escape sequences<sup>13</sup>. These included preparatory wing raising (Fig 1b, purple) and ‘takeoff’; the latter consists of rapid extension of both middle legs (which would result in a jump in non-tethered flies<sup>6</sup>) followed by flight initiation (Fig 1b, blue). In flying flies, the same looming stimulus evoked robust landing responses (Fig 1b, orange, Supplementary videos 1 and 2), in which all six legs simultaneously extend away from the body in preparation for impact<sup>14,15</sup> (Supplementary video 3). Some trials included a takeoff followed by a landing response. Thus, escape and landing responses, which comprise completely different motor patterns, can be triggered by the same looming stimulus. As expected, selection of the two behaviors depended entirely on the fly’s behavioral state – landing responses were only evoked in flight, whereas escape-related leg movements were only evoked in non-flying flies (Fig. 1c, note automatic landing detection yielded false positives related to grooming in three perching flies). We conclude that the sensorimotor pathways for landing and escape have an overlapping sensory parameter space, such that information about the behavioral state, in this case flight vs. non-flight, must be integrated with sensory information to select the appropriate action.

## Two identified DN types contribute to landing responses

To understand the mechanisms by which information about the behavioral state is integrated in the selection of escape or landing responses, we first set out to determine at which stage in the neural processing of information — from visual sensory circuits in the brain to motor networks in the ventral nerve cord (VNC) — neural commands for landing and escape are distinguished. As described above, the sensorimotor pathway controlling looming-evoked takeoff in *Drosophila* is known and includes the Giant Fiber DNs<sup>4–6,16</sup>. However, the neural circuits that control landing were unknown in any animal. To determine if there are distinct DNs for landing control, we optogenetically activated 133 *Drosophila* split-GAL4 driver lines targeting individual DN types<sup>17</sup> during tethered flight and monitored behavioral responses. Only two DN types, DNp07 and DNp10 (Fig. 1d), drove landing-like extensions of all six legs when activated (Fig. 1e, Supplementary videos 4 and 5). DNp07 and DNp10 types each comprise a bilaterally symmetric pair (one left, and one right copy) of morphologically identifiable neurons with cell bodies on the brain's posterior surface. The DNp07 and DNp10 dendrites overlap the bundled axon terminals of visual projection neuron types LPLC3 and LPLC4<sup>17</sup>, which form optic glomeruli in the central brain (Supplementary Figure 1a–c). The LPLC3 and LPLC4 glomeruli reside near the glomeruli of two other visual projection neuron types (LPLC2 and LC4), which are known to encode visual looming features and synapse directly onto the Giant Fiber<sup>3–5</sup>. DNp07 and DNp10 axon terminals primarily form output synapses in all six VNC leg neuropils, where the leg motor control networks reside (Fig. 1d, Supplementary Figure 1; see also<sup>17</sup>). Their anatomy therefore suggests that both DNp07 and DNp10 integrate visual information to drive movements of all legs.

We used a combination of manual and machine-vision based methods to track the movements of the leg tips in high-speed video during optogenetic activation of DNp07 or DNp10 as well as during visual stimulation (Fig. 1e, Supplementary Figure 2). Leg kinematics in both conditions were very similar, and met the previously-defined criteria for a landing response<sup>7,14,18</sup>: simultaneous extension of all legs with the front legs reaching beyond the head. The latency from the start of optogenetic activation to the first video frame of leg movement was short for both DN types (DNp10,  $21 \pm 4$  ms; DNp07,  $26 \pm 5$  ms;  $N = 7$  flies,  $n = 21$  trials each DN during flight; Figure 1e, Supplementary videos 6 and 7). Together with the DN innervation of leg motor neuropils, this suggests relatively direct connections from the DNs to motor neurons. DNp10 activation directed the middle and hind legs more laterally than DNp07 (Supplementary Figure 3), such that the motor patterns driven by the two DN types were similar to each other, but not identical.

To test whether DNp07 and DNp10 are necessary for normal expression of visually-evoked landing responses, we used DN-specific split-GAL4 lines to silence each DN type by targeted expression of Kir2.1 channels<sup>19</sup> and exposed flies to repeated frontal looming stimuli. We quantified each fly's landing response rate by automatic detection of large-amplitude front leg extensions (Supplementary Figure 4). Control flies expressing GFP in DNp07 or DNp10 (Supplementary videos 1 and 2) and most control flies driving Kir2.1 under the empty-split-GAL4 construct, which has no expression in the central nervous system, exhibited full landing responses to over 75% of looming stimuli. Compared to

control flies, DNp07- or DNp10-silenced flies showed significantly reduced landing response rates to frontal looming stimuli, and often exhibited no or small-amplitude leg extensions (Fig. 1f, DNp10-split-GAL4, 37% median reduction in landing rate; DNp07-split-GAL4-1, 46%; see also Supplementary Figure 4, Supplementary videos 8 and 9). Flies in which DNp07 was silenced using a second driver line (DNp07-split-GAL4-2) did not exhibit significantly reduced landing response rates to looming compared to the empty-split-GAL4>UAS-Kir2.1 control, likely due to weaker expression levels. However, silencing DNp07 or DNp10 using either line significantly reduced landing response rates to unilateral, front-to-back moving bars (Figure 1f, DNp10-split-GAL4: 41% median reduction in landing probability, DNp07-split-GAL4-1: 35%, DNp07-split-GAL4-2: 36%). We used these stimuli subsequently to physiologically characterize DN visual responses. In contrast, takeoff response rates to looming remained unimpaired after silencing either DN type (Supplementary Figure 4d). Thus, DNp07 and DNp10 are required for full expression of visually-evoked landing responses but not for takeoff.

The variability of landing response rates in DN-silenced flies was relatively high (Figure 1f, Supplementary Figure 4e). Some DN-silenced flies barely responded to visual stimuli (Supplementary videos 8 and 9), and thus had response rates similar to L1/L2-silenced flies, which cannot see visual motion and therefore served as negative controls (Figure 1f). Other individuals had response rates similar to the positive controls (Figure 1f, Supplementary video 10). This variability was not entirely unexpected, given that we silenced only one of the two DN types that can drive landing in each experiment, leaving the other DN type unaffected.

### **DNp07 and DNp10 spike rate controls visually-evoked landing response amplitude**

To test if DNp07 and DNp10 respond to visual stimuli and control landing leg movements on a moment-to-moment basis, we next quantified their activity using *in vivo* whole-cell patch-clamp recordings in head-fixed, behaving flies (Fig. 2a). Landing responses can be evoked by both frontal looming<sup>7</sup> and its unilateral approximation, front-to-back edge motion (Fig. 1e). We presented visual stimuli unilaterally to enable high-speed video recordings for leg tracking from the other side of the fly (Fig. 2a). In these experiments, we ablated the front legs to avoid interference with visual stimulation and recordings. Ipsilateral, front-to-back moving dark bars drove both DN types most strongly. Contralateral stimuli, smaller moving objects, lateral looming, movements in other directions, and bright progressive edge motion were less effective (Fig. 2b–e, Supplementary Figure 5). DNp07 had stronger contralateral visual responses than DNp10 (Supplementary Figure 5a, f), possibly affording DNp07 symmetric drive to ipsi- and contralateral leg motor networks despite having more asymmetric axonal projections than DNp10 (Figure 1d). A cross-correlation between spiking activity and leg movements indicated that visually-driven spiking preceded leg movements in both DN types (Fig. 2f). In addition, both the first spike and the peak spike rate consistently preceded the onset of leg movements for both DN types (Supplementary Figure 6). Together with the optogenetic activation results, this strongly suggests that spiking in DNp07 and DNp10 causes leg movements, and not vice-versa.

Although previous studies suggest the landing response is an all-or-none reflex<sup>20</sup>, we found that DN spike rate correlated with leg extension amplitude (Fig. 2g, Supplementary Figure 6). Thus, visual stimuli eliciting the highest spike rate also drove the largest leg extensions (Fig. 2h–i). To confirm a causal relationship between DN spike rate and leg extension amplitude, we calibrated our optogenetic stimulation (Supplementary Figure 7) to be able to drive controlled spike rates in each DN type. In optogenetic activation experiments, the spike rate of each DN type determined leg extension amplitude (Fig. 2j–k). We note that leg extension amplitudes continued to increase with artificial activation of a single cell type beyond spike rates typically observed during visual stimulation (estimated spike rates >150 Hz, Fig. 2k). This is consistent with leg extension amplitude being driven by both DNp07 and DNp10, if they are activated simultaneously during visually-evoked landing responses, to achieve maximum extension. If a downstream circuit sums their combined spike rates to set the leg amplitude, activating one DN type artificially at a high rate while the other is silent, would mimic the natural co-activation of both DN types.

Based on our *in vivo* recordings, we suggest that DNp07 and DNp10 are most responsive to visual stimuli derived from fast, dark objects approaching from the front, which matches the behavioral tuning of landing responses<sup>7,8</sup> (see also Fig. 2i), and that co-activation of DNp07 and DNp10 by these stimuli controls landing leg extensions on a moment-to-moment basis. Synergistic control of landing by DNp07 and DNp10 is also supported by our silencing experiments, in which visually-induced landing response rates were reduced, but not abolished, when one of the two DN types was silenced. Our data do not preclude the existence of descending neurons other than DNp07 and DNp10 that contribute to visual landing control, nor do they rule out participation of DNp07 and DNp10 in other flight behaviors involving leg movements, such as steering<sup>21</sup>. However, they do establish these two cell types as significant contributors to the endogenous control of visually-evoked landing. We thus subsequently refer to DNp07 and DNp10 as ‘landing DNs.’

### Visual responses of landing DNs are gated by behavioral state

Having ascertained that takeoff and landing behaviors can be triggered by the same visual stimulus, but are controlled through distinct DN populations, we next used the landing DNs to investigate whether information about the behavioral state is integrated with visual information at the DN level. To this end, we recorded landing DN responses to the same set of visual stimuli used previously, this time comparing flight and non-flight periods. Visual responses of both DN types were highly flight-dependent (Fig. 3a–c). Supra-threshold visual responses were completely eliminated without flight in DNp10 for all visual stimuli tested. In non-flight trials, DNp07 visual responses were reduced below the spike rates required to elicit leg movements in activation experiments (e.g. 70% reduction in spike rate, from 92 to 27 Hz, for 1000 °/s fast bars; Fig. 3a–c).

To test if this permissive gating of landing-DN responses by flight was modality specific or general, we puffed an airstream over non-flying flies to broadly stimulate mechanoreceptors (Fig. 3d). Both landing DNs responded to mechanosensory stimulation and were thus multimodal (Fig. 3d–f). DNp10 was excited by air puffs, which drove strong spike responses, whereas DNp07 was inhibited strongly enough to reduce spiking (Fig. 3d).

Importantly, unlike for visual stimuli, the response of DNp10 to mechanosensory stimuli did not require flight. This suggests that information about the behavioral state specifically gates the responses of landing DNs to visual stimuli, such that visually-evoked spike rates are reduced below the activity levels required for landing responses during non-flight bouts, when the motor program they drive would be deleterious.

To determine if additional, downstream mechanisms<sup>22,23</sup> contributed to the gating of landing responses at the level of the VNC, we optogenetically activated DNp07 and DNp10 in non-flying flies. Activation of either DN reliably induced landing-like extensions of all six legs (24/24 trials, N = 4 flies and n = 12 trials per DN, Supplementary videos 6 and 7), as during flight trials. This suggests that behavioral-state dependent gating occurs at the DN dendrites or in upstream sensory circuits of the brain, without additional downstream gating mechanisms in the VNC. In addition to landing-like leg extensions, artificial activation of landing DNs in non-flying flies often resulted in flight starts at a longer latency. For DNp07, mean ( $\pm$  SD) latencies to leg movement onset were  $16 \pm 4$  ms (n = 12 trials) compared to  $73 \pm 29$  ms to the start of flight (n = 10 trials), and for DNp10, latency to leg movement onset was  $15 \pm 4$  ms (n = 12 trials) compared to  $50 \pm 16$  ms to the start of flight (n = 12 trials). Since flight starts had much longer latencies and were less reliable than leg movements, we suspect the former resulted either from secondary startle responses to DN activation or from indirect, polysynaptic connections between landing DNs and flight motor circuits.

As further confirmation that landing DN activity did not correlate with other leg movements in non-flying flies, we quantified DN spike rates in a 1-s pre-stimulus interval before all ipsilateral front-to-back moving bar stimuli during non-flight bouts. In these periods, leg movements varied and included grooming, air-walking or quiescence. Under these conditions, spiking was almost completely absent in both DN types. DNp07 had a mean  $\pm$  SD spike rate of  $0.017 \pm 0.06$  Hz (N = 6 flies, n = 331 trials), and DNp10 had a mean  $\pm$  SD spike rate of  $0.003 \pm 0.017$  Hz (N = 6 flies, n = 308 trials, only one spike was detected in all trials combined). In contrast, both DN types readily reached spike rates exceeding 50 Hz during visual stimulation in flight. This indicates that the landing DNs do not drive or respond to non-landing leg movements.

### The two landing DN types receive behavioral-state information through separate mechanisms

How is the behavioral state conferred to the landing DNs to gate visual responses? Octopamine (OA) — the insect analogue of norepinephrine — is released during flight, and both its bath application and release by activation of central neuromodulatory neurons can mimic the flight state and increase responses of visual interneurons<sup>24–26</sup>. To determine if gating of landing DNs was mediated by OA, we bath-applied OA in non-flying flies and recorded DNp07 (Fig. 4a–b) and DNp10 (Fig. 4c–d) responses to visual stimuli. DNp07 more than doubled its average non-flight visual response after OA application (Fig. 4b), and this effects was significant (Fig. 4e; Wilcoxon rank-sum test,  $p < 0.001$  at  $1000^\circ/\text{s}$ , N = 5 flies, n = 29 trials before and n = 44 trials during OA application), indicating visual responses in DNp07 are gated by octopaminergic modulation. In contrast, OA application had no effect on DNp10 visual responses (Fig. 4c–e,  $p = 0.24$  at  $1000^\circ/\text{s}$ , N = 7 flies, n = 45

trials before and  $n = 71$  trials during OA application). Thus, neuromodulation by OA is responsible for gating only one of the two DN types. Apart from OA, dopamine (DA) is implicated in locomotor state-dependent modulation in flies<sup>27</sup>. We tested whether bath application of DA affected DNp10 visual responses and found that like OA, DA did not increase DNp10 visual responses in non-flying flies (Supplementary Figure 8).

Since the two strong neuromodulator candidates implicated in mediating flight dependence did not affect DNp10, we hypothesized that flight-state information is conferred to DNp10 through a different mechanism. We observed that DNp10 was tonically depolarized during flight and quickly repolarized at flight cessation, whereas the DNp07 baseline membrane potential was not affected by flight (Fig. 4f). This suggested that DNp10 receives direct, flight-related excitatory inputs, either from externally-generated refferent feedback from mechanoreceptors stimulated during flight<sup>23,28</sup> or through internal feedback signals from the flight motor circuit<sup>29</sup>.

Flight-related refferent feedback onto DNp10 could potentially derive from its excitatory mechanosensory inputs (Fig. 3d–f). Ablation experiments revealed that in non-flying flies DNp10 responses to wind stimulation were entirely driven by mechanoreceptors on both antennae (Supplementary Figure 9). In *Drosophila*, the antennae are known to be stimulated during flight and provide feedback to the flight-control circuitry<sup>28</sup>, which made them good candidates for providing refferent feedback to DNp10. Mechanosensory inhibition of DNp07, in contrast, was mediated by mechanoreceptors on both the antennae and legs (Supplementary Figure 9). However, ablation of the antennae did not affect DNp10's flight-dependent increase in visual responses or its flight-dependent baseline depolarization (Fig. 4g). Ablation of other flight-related mechanoreceptors on the wings and halteres also had no effect on DNp10 visual responses or its flight-dependent depolarization (Fig. 4g). The observation that none of the candidate mechanoreceptors mediated the flight-dependence of DNp10 indicates that gating of DNp10 does not occur through refferent feedback from the primary flight-related mechanoreceptors, which leaves internal feedback signals from the flight motor circuit as the most likely mechanism gating DNp10 visual responses.

## Discussion

Taken together, our data show that DNp07 and DNp10 receive information about the behavioral state of the animal through different mechanisms. This state information gates responses of both DN types to visual stimuli, which determines the expression of landing behavior. Our results thus show that gating of DN activity is the mechanism underlying a critical real-world choice: how to respond to a looming stimulus, when visual cues alone are ambiguous as to whether the animal is approaching the object or vice versa. Context-dependent changes in neural activity are ubiquitous in the animal kingdom<sup>30</sup>, and modulation or gating of DN activity by locomotor state has been observed in insects<sup>31–35</sup> and vertebrates<sup>36</sup>, indicating that such gating may be a general mechanism by which nervous systems effect adaptive behavioral choices.

The gating of DN activity we observe is modality specific and thus does not occur through general inhibition of the landing DNs during non-flight periods, as might be expected from

established action selection mechanisms, such as reciprocal inhibition<sup>37</sup>. Rather, visual information is specifically coupled to the landing DN pathways by two separate mechanisms (Supplementary Figure 10). Gating of DNp07 activity is mediated by neuromodulation of the sensorimotor circuit through OA, which could occur in visual circuits presynaptic to DNp07<sup>26,38,39</sup>, locally at the level of the DN itself, or both. Gating of DNp10 activity, on the other hand, is most likely achieved by direct feedback from flight motor circuits onto the DN itself, which would explain the tonic depolarization of DNp10 during flight (Supplementary Figure 10). This feedback could, for example, be provided by ascending neurons that project from the flight motor circuit in the VNC directly onto DNp10 dendrites in the brain or gnathal ganglion<sup>29</sup>. The presence of multiple, distinct coupling mechanisms acting on separate DN types potentially confers robustness and finer control to the system. For example, since each landing DN drove a slightly different angle of leg extension when activated (Supplementary Figure 3), differential gating of the two landing DN types could potentially be used to adopt different landing postures as required for landing on different substrates or surface orientations.

State-dependent coupling could also enable the same computed visual features to be used in multiple behavioral circumstances, for example during walking<sup>40</sup>, courtship<sup>41,42</sup>, or flight<sup>11</sup>, by rendering responsive only the subset of DNs that control contextually appropriate actions. In the current understanding of fly visual processing, looming is detected by specific visual projection neuron types from the optic lobe that distribute computed looming-feature information to several of the nearly 20 optic glomeruli in the central brain<sup>1-4</sup>. DNs for takeoff and landing differentially innervate subsets of the optic glomeruli<sup>4,5,17</sup>. Our results suggest that flexibility is added to this wiring scheme by coupling or decoupling the DNs from visual inputs depending on the animal's current behavioral state (Supplementary Figure 10). This is clearly the case for landing DNs, in which visual responses are suppressed in non-flight states. Our behavioral data suggests that descending neurons for escape, such as the Giant Fiber and parallel escape DNs<sup>43</sup>, may conversely be decoupled from visual inputs during flight (Supplementary Figure 10), since escape motor patterns, such as rapid middle leg extensions driving escape jumps, did not occur in response to looming stimuli in flight trials (Fig. 1b-c, Supplementary videos 1 and 2).

The optic glomeruli encode visual features used in a wide range of fly visual behaviors<sup>1</sup>, and nearly 20% of the known DN population directly innervate these areas<sup>17</sup>. Vertebrate nervous systems similarly organize visual input into encoded features<sup>44</sup> and link these to distinct motor actions through descending pathways<sup>45</sup>. This suggests that state-dependent gating of DN activity could be a general principle by which nervous systems flexibly couple sensory features to motor pathways in order to rapidly select an appropriate action.

## Methods

### Fly Stocks

All *Drosophila melanogaster* stocks were reared on a 16h/8h light/dark cycle at 22–25°C and 50% humidity on standard cornmeal fly food, and used for experiments 3–5 days after eclosion. For optogenetic activation experiments, larval flies were raised on standard cornmeal food plus 0.2 mM retinal and switched to standard food plus 0.4 mM retinal upon

eclosion. These fly vials were kept in the dark until flies were prepared for experiments. All experiments were performed on female *Drosophila melanogaster*.

We used split-GAL4<sup>46</sup> lines expressing GFP or CsChrimson<sup>47</sup> in DNp10 or DNp07 for patch-clamp and optogenetic activation experiments. An empty-split-GAL4 line, with no expression in any neurons or muscles, crossed to the CsChrimson effector line was used as a control for optogenetic activation (Fig. 2j). These flies did not show landing responses to LED pulses used for optogenetic activation experiments.

### Fly genotypes

The following parental fly lines were used to generate experimental flies for the data presented in this study:

DNp10-split-GAL4 (SS01608): VT031084-p65ADZp (attP40); 48E11-ZpGDBD (attp2)<sup>17</sup>

DNp07-split-GAL4–1 (SS02276): VT 029814-p65ADZp (attP40); VT047755-ZpGDBD (attp2)<sup>17</sup>

DNp07-split-GAL4–2 (SS01549): VT029814-p65ADZp (attP40); VT003280-ZpGDBD (attp2)<sup>17</sup>

L1–L2-split-GAL4 (SS00797): R48H08-p65ADZp (attP40); R29G11-ZpGdbd (attP2)<sup>48</sup>

empty-split-GAL4 (SS01062): R24A03-p65ADZp (attP40); R74C01-ZpGDBD (attP2)<sup>17</sup>

UAS-GFP: pJFRC28–10XUAS-IVS-GFP-p10 (attP2)<sup>6,46</sup>

UAS-CsChrimson: 20XUAS-CsChrimson-mVenus (attP18)<sup>47</sup>

UAS-Kir2.1: w+;;pJFRC49–10XUAS-IVS-eGFPKir2.1 (attP2)<sup>6,49</sup>

DNp07-split-GAL4–2 was used for activation experiments shown in Figure 1e and Supplementary Figure 3, and Supplementary video 1, and also in one set of silencing experiments in Figure 1f. DNp07-split-GAL4–1 was used for all other experiments. We used two different DNp07 lines to make sure that the phenotypes associated with DNp07 were not due to faint expression in a second descending neuron that does not target leg neuropils in DNp07-split-GAL4–1. GFP expression was also brighter in DNp07-split-GAL4–2, perhaps suggesting DNp07-split-GAL4–2 had higher expression levels than DNp07-split-GAL4–1.

### Anatomy

The anatomical methods are described in detail by Namiki et al.<sup>17</sup>. In brief, DN specific driver lines expressing GFP or CsChrimson-mVenus were imaged with confocal microscopes using Janelia FlyLight standard protocols (<https://www.janelia.org/project-team/flylight/protocols>). MultiColor FlpOut<sup>50</sup> was used to unilaterally label individual neurons (Fig. 1d, Supplementary Figure 1). In order to overlay the two DNs in the same image (Fig. 1d, Supplementary Figure 1), brains were aligned to the JFRC2013 standardized brain template (<https://github.com/jefferislab/BridgingRegistrations>), and VNC image data were aligned to a template imaged by the FlyLight Project team (<https://github.com/>

[VirtualFlyBrain/DrosAdultVNSdomains/blob/master/template/Neuropil\\_185.nrrd](#)), as described earlier<sup>17</sup>. The following antibodies were used for staining: AF488 Goat anti Rabbit concentrated 1:400 (Life Technologies, Thermo Fisher Scientific, Cat# A-11034; RRID: AB\_2576217), AF568 Goat anti Mouse concentrated 1:400 (Life Technologies, Thermo Fisher Scientific Cat# A-11031; RRID: AB\_144696), nc82 Mouse anti bruchpilot concentrated 1:30 (Developmental Studies Hybridoma Bank, DSHB Cat# nc82; RRID: AB\_2314866), Rabbit polyclonal anti GFP Fraction concentrated 1:1000 (Life Technologies, Thermo Fisher Scientific Cat# A-11122; RRID: AB\_221569). These antibodies and protocols have been validated for this species and application<sup>17</sup>.

## Electrophysiology

Patch clamp recordings in behaving flies were achieved using previously described methods<sup>6,38</sup>. In brief, female flies were anesthetized at 4°C on a cold plate, and mounted on a pyramidal fly holder using UV-glue. Front legs were removed, to eliminate interference with recordings and visual stimulation, and a small hole was cut into the cuticle on the posterior surface of the head to expose the brain in the region of the targeted cell body. The brain was continuously perfused with fly extracellular saline (103 mM NaCl, 3 mM KCl, 5 mM *N*-Tris (hydroxymethyl)methyl-2- aminoethane-sulfonic acid, 8 mM trehalose, 10 mM glucose, 26 mM NaHCO<sub>3</sub>, 1 mM NaH<sub>2</sub>PO<sub>4</sub>, 1.5 mM CaCl<sub>2</sub> and 4 mM MgCl<sub>2</sub>, adjusted to 273–275 mOsm, pH 7.3) held at 22°C and bubbled with 95% O<sub>2</sub>/5% CO<sub>2</sub><sup>6,51</sup>. Collagenase (5% or 2.5% in extracellular saline) was locally applied with a blunt patch-pipette to disrupt the perineural sheath surrounding the brain and render the tissue penetrable. DNp07 or DNp10 neurons were recorded on either side of the brain, using electrodes with tip-resistances between 5 and 10 MΩ, filled with intracellular saline (140 mM potassium aspartate, 10 mM HEPES, 1 mM EGTA, 4 mM MgATP, 0.5 mM Na<sub>3</sub>GTP, 1 mM KCl, 20 μM Alexa-568-hydrazide-Na, adjusted to 260–275 mOsm, pH 7.3). Recordings were accepted for analysis if a seal resistance > 4 GΩ was achieved before breaking in, spike amplitudes were >30 mV for DNp07 and >5 mV for DNp10, and if the resting membrane potential in the non-flight state was <−60mV. In DNp07, spikes could be evoked by moderate current injections (50 pA), which was not possible in DNp10. For visual stimulation, recordings were only included in the analysis if a full data set of looming, moving squares and moving bars was recorded during both flight and non-flight. This corresponded to 15 different stimuli, with four repetitions for each condition. Recordings thus needed to be stable for at least 30 minutes to be included in the analysis of visual responses. No holding current was injected throughout. Flies were induced to fly by applying gentle air puffs. Flies stopped flying either spontaneously or when presented with a pipette tip to grasp. Flight- and non-flight bouts were interleaved. Recordings were acquired in current clamp mode with a MultiClamp 700B amplifier (Molecular Devices, Sunnyvale, CA), low-pass filtered at 10 kHz, and digitized (Digidata 1440A, Molecular Devices, Sunnyvale, CA) at 20 kHz. Intracellular traces in figures were corrected for a 13-mV liquid junction potential<sup>51</sup>.

## Optogenetic activation

For optogenetic activation, we used a 625-nm Fiber-Coupled LED with 1-mm Fiber Patch cable (Thorlabs, Newton, NJ) pointed directly at the fly from below. The light penetrated the

cuticle from the same location in both behavior and electrophysiology experiments, allowing direct comparison of our data sets. DN spike responses to CsChrimson stimulation were almost identical in flight and non-flight trials (Supplementary Figure 11). The LED was controlled by a T-cube LED driver (Thorlabs, Newton, NJ), on which the power level was manually selected. The LED was triggered via a data acquisition board (NI-DAQ, National Instruments, Austin, TX), controlled by custom written Matlab code. See Supplementary Figure 7d for light intensities used. Light pulses were 300-ms long in the experiments shown in Fig. 1, and 50-ms long in all other experiments.

### Fly behavior experiments

For the behavioral experiments shown in Fig. 1b,c and f, and Supplementary Figure 4, flies were anesthetized at 4°C on a cold plate and tethered to a pin on the dorsal thorax, so that the head and legs could move freely. They were mounted in the center of a cylindrical blue LED display<sup>31,52,53</sup> (470-nm peak wavelength), spanning 216° of the visual field in the horizontal, and 72° in the vertical dimension. Each pixel covered 2.25° of the fly's visual field in the center of the display. For visual stimulation, we used looming stimuli ( $r/v = 80$  ms) centered in the fly's frontal visual field, and bars moving front-to-back unilaterally at 500°/s. The looming stimulus used four different brightness values to interpolate the edge pixel intensity and thus create smooth circular outlines. For behavioral analysis, we used a Wingbeat Tachometer (IO Rodeo, Pasadena, CA) and three cameras filming the flies at 100 Hz (maximal acquisition rate) from below and both sides (Supplementary videos 1, 2 and 6–8). Leg movement ROIs were defined in a custom-written interface<sup>31</sup>. The ventral view was used to define an ROI for front legs extension (Supplementary Figure 4). ROI position was adjusted for each fly. Mean ROI intensities were calculated in real time, fed into a digitizer (Digidata 1440A), and recorded at 20000 Hz alongside the videos and Wing beat Tachometer traces. The mean ROI intensity values were low-pass filtered (50-ms time window) and thresholded to acquire timestamps for leg extensions. The threshold was defined as 3x the standard deviation for any given trace. Events in the escape response were defined by wing beats, with singular, isolated wing beat signals defined as wing raising events, and the first wing beat of a flight bout as takeoff. We inspected the videos alongside the recorded wing beat data to validate our behavior classifications.

In a separate set of experiments (Fig. 1e, Supplementary videos 4 and 5), flies were tethered in the same way, but DNs were activated optogenetically (see above). Flies were filmed from below using a Photron SA4 camera at 125 frames per second. The video of a fly landing spontaneously during free flight (Supplementary video 3) was captured serendipitously in our FlyPEZ behavioral apparatus<sup>54</sup>.

In all other behavioral experiments, flies were tethered to the same pyramidal holder used in electrophysiology experiments and filmed from the side at 1000 Hz using an SA4 high-speed video camera (Photron, San Diego, CA). Images and electrophysiology data were synchronized using a TTL trigger signal, and a copy of the electrophysiological recordings was synchronously acquired through the camera's MCDL board (Photron, San Diego, CA). Flies were illuminated by two infrared (850 nm) LEDs and the wing beat frequency was monitored with a Wingbeat Tachometer. For experiments without patching, flies were

tethered as for electrophysiological recordings, but front legs were left intact and the head cuticle was not incised.

### Visual stimulation in electrophysiology experiments

Visual stimuli were back-projected at  $768 \times 768$  resolution onto a 7-inch diameter hemisphere coated with rear projection paint (ScreenGoo, Goo Systems Global, Ontario, Canada). We used a DMD projector running at 360 Hz with the color wheel removed (developed by A. Leonardo and Lightspeed Design; model WXGA 360), driven by MATLAB (Mathworks, Natick, MA) using the Psychophysics Toolbox<sup>55</sup>. For the data shown in Supplementary Figure 4I, we used a similar setup with two projectors creating bilateral stimuli on two domes.

We analyzed neural responses to five visual stimulus types:  $10^\circ$  wide dark bars,  $10 \times 10^\circ$  small dark squares, dark looms, and dark and bright edges. Bars and squares moving from front to back across the visual field were presented at five different speeds to quantify the speed tuning of landing DNs (10, 50, 100, 500,  $1000^\circ/\text{s}$ ). Moving squares were positioned at the equator of the visual field; bars extended the entire length of the screen. Additionally, bars and squares were presented moving at  $100^\circ/\text{s}$  in four directions (front to back, back to front, upwards, downwards) to characterize directional selectivity. Dark, looming disks were presented at  $45^\circ$  azimuth and  $45^\circ$  elevation and expanded from  $5^\circ$  to  $90^\circ$  at different size to speed ratios (radius/velocity,  $r/v$ <sup>56</sup>) of 10, 40, 70, 100 and 140 ms. Each stimulus was presented at least four times during flight and non-flight bouts. Visual stimuli were randomized, and the interstimulus-interval was 10 s. To measure the contrast-selectivity of both landing DNs, dark or bright edges were presented moving from front to back at  $500^\circ/\text{s}$ . This stimulus protocol only contained these two stimuli, and their order was randomized.

### Mechanosensory stimulation

Flies were exposed to one-second long air puffs to the entire body, generated with a Picospritzer III (Parker, Hollis, NH), delivered from a postero-lateral direction via a thin-walled glass capillary. The air puffs were quite strong, such that the antennae, wings, and legs were moved by the airstream. However, the air puffs did not initiate flight. The stimulus was designed to broadly stimulate mechanoreceptors, so that specific conclusions about mechanosensory inputs to the DNs could be drawn through ablation experiments.

### Pharmacology

To test for an effect of Octopamine (OA) on the visual responses of landing DNs, we first measured visual responses in regular saline, as a baseline, and then washed in saline containing 1.6 mM OA (Sigma-Aldrich, Saint Louis, MO) for at least 20 minutes before measuring the responses to the same visual stimuli. This relatively high OA concentration<sup>25,57</sup> was used to ensure that the lack of an effect of OA on DNp10 visual responses was not due to a low final concentration in the saline and at the neuron's dendrites. The same protocol was used for Dopamine (DA) application. DA-Hydrochloride (Sigma-Aldrich) was concentrated at 10 mM in regular saline, and 50  $\mu\text{M}$  Sodium-Metabisulfite (Sigma-Aldrich) was added to prevent the DA from oxidizing. DA solution

was made fresh directly before washing it in, and we used two different DA batches to rule out that the DA was contaminated or inactive for other reasons.

### **Spike detection**

Because of the different morphologies of the two landing DNs, spikes recorded in the soma of DNp07 were about 4 times larger than in DNp10. We therefore used a flexible spike detection script that could be used for both cell types. Recordings were temporally smoothed (0.35 and 0.7 ms windows for DNp07 and DNp10, respectively), and a threshold was applied to the derivative of the recording to detect fast positive slopes. Accurate spike detection was confirmed by inspection of the raw membrane potential plotted alongside the detected spike times for several seconds at the beginning, the middle, and the end of the recording (see Supplementary Figure 7b for an example).

### **Quantification of DN visual responses**

Visual responses were calculated as mean spike rates, computed within a window starting at stimulus onset and ending 50 ms after the stimulus disappeared from the screen, or stopped moving (in the case of looming stimuli). For directional tuning curves, we computed the mean peak spike rate in 20-ms bins during the same interval. Spike rates were averaged for each fly, over a minimum of four trials.

### **Quantification of flight-dependent membrane potential changes**

To test whether the DN membrane potential was affected by behavioral state, we calculated flight-dependent changes in membrane potential as the membrane potential difference between the last 500 ms of every flight bout and a 500-ms-long window after flight, when the membrane potential had returned to baseline (gray boxes in Figure 4).

### **Quantification of DN responses to optogenetic activation**

Like responses to visual stimulation, responses to DN activation were calculated as mean spike rates, computed within a window starting at stimulus onset and ending 50 ms after stimulus offset. Note that spike rates are not directly comparable between visual and optogenetic activation. While we chose the same window to compute mean responses, DN responses to optogenetic activation had a much shorter delay, and lasted longer than responses to visual stimulation, resulting in much higher spike rates in the 100-ms window used for analysis.

### **Leg tracking**

We developed a machine-learning-based method to track the tips of the fly's legs in a side-view of the fly captured simultaneously with the patch-clamp recordings. We manually positioned landmark points on the fly's legs in a subset of video frames, then used a modified version of the Cascaded Pose Regression (CPR) algorithm<sup>58</sup> to learn a regression function which inputs a single video frame and outputs a prediction of the  $(x,y)$ -locations of the landmarks in that frame. CPR begins by randomly choosing initial guesses of the landmarks' positions. Then, it iteratively applies a cascade of random fern regressors<sup>59</sup> to update the estimates of the landmarks based on image features extracted from the video

frame. These image features are extracted from locations in the image relative to the previous estimate of the landmarks' positions. The CPR learning algorithm selects regression parameters so that each layer of the cascade predicts updates to the landmarks' positions that match the manually labeled data as well as possible. We used an interactive framework to iteratively train the algorithm, then find frames on which the previous version of the tracker was failing, manually relabeling these frames, and restarting the process. In total, our tracker was trained on 246 Videos from 15 flies. After training, we ran the CPR tracker on every frame of every video, and manually inspected and corrected the results. The same labeling environment was used to manually label the tip positions in six-legged flies. We excluded the contralateral middle and hind legs from the analysis because they were frequently covered by the fly's thorax, abdomen, or ipsilateral legs. The tracking software is available at <https://github.com/kristinbranson/APT>.

### Correlations of DN activity and leg movement

In order to test whether landing DNs contributed to visually evoked leg movements in behaving flies, we analyzed the timing and magnitude of DN activity in relation to leg movements. Since front legs were ablated in patch-clamp experiments, middle legs were used as a proxy for leg motion. This simplification was reasonable since the middle and front legs move in-phase with each other during the landing response (Supplementary Figure 2). For calculating the cross-correlation, both the intracellularly recorded spike rates and leg movement traces were binned every 100 ms. Both traces were normalized to their respective peak value and thus ranged from 0 to 1. For Figure 2g and h, mean spike rate was calculated in a window from 500 ms before to 200 ms after peak leg extension.

### Statistics

We used standard statistical tests to evaluate our data, and the results are reported at the relevant locations in the text or figure captions. Statistics were computed in MATLAB. No statistical methods were used to pre-determine sample sizes but our sample sizes are similar to those reported in previous publications<sup>6,26,31</sup>. We mainly used non-parametric statistical tests. Where t-tests were used, data distributions were assumed to be normal, but this was not formally tested. Data collection and analysis were not performed blind to the conditions of the experiments. Stimulus presentation was randomized in electrophysiological experiments, and flight and non-flight trials were interleaved. In behavioral experiments, visual stimuli were presented in a fixed, interleaved order (1, 2, 3, 1, ...). We did not exclude any data sets from the analysis that matched the criteria for minimal number of trials required and recording quality, as defined above. Please see the Life Sciences Reporting Summary for further details.

### Supplementary Material

Refer to Web version on PubMed Central for supplementary material.

### Acknowledgements

We thank K. von Reyn, M. Peek, and S. Huston for sharing their rigs and providing software, M. Dickinson, and T. Lindsay for building the Kinefly setup, M. Sumathipala, D. Parikh, and P. Breads for labeling fly videos, and W.

Korff and the Janelia Descending Interneuron Project for help with the DN split-GAL4 screen. We are grateful to G. Zheng and the Janelia Fly Core for fly husbandry, and to E. Gruntman and M. Reiser for sharing LED-arena code and advice. V. Jayaraman, K. Longden, E. Gruntman, C. Dallmann and Card lab members provided helpful comments on the manuscript. This study was supported by the Howard Hughes Medical Institute.

## References

1. Wu M et al. Visual projection neurons in the *Drosophila* lobula link feature detection to distinct behavioral programs. *Elife* 5, (2016).
2. Panser K et al. Automatic Segmentation of *Drosophila* Neural Compartments Using GAL4 Expression Data Reveals Novel Visual Pathways. *Curr. Biol* 26, 1943–1954 (2016). [PubMed: 27426516]
3. Klapoetke NC et al. Ultra-selective looming detection from radial motion opponency. *Nature* 551, 237–241 (2017). [PubMed: 29120418]
4. von Reyn CR et al. Feature Integration Drives Probabilistic Behavior in the *Drosophila* Escape Response. *Neuron* 94, 1190–1204 (2017). [PubMed: 28641115]
5. Ache JM et al. Neural Basis for Looming Size and Velocity Encoding in the *Drosophila* Giant Fiber Escape Pathway. *Curr. Biol* 29, 1073–1081.e4 (2019). [PubMed: 30827912]
6. von Reyn CR et al. A spike-timing mechanism for action selection. *Nat. Neurosci* 17, 962–970 (2014). [PubMed: 24908103]
7. Tammero LF & Dickinson MH Collision-avoidance and landing responses are mediated by separate pathways in the fruit fly, *Drosophila melanogaster*. *J. Exp. Biol* 205, 2785–2798 (2002). [PubMed: 12177144]
8. van Breugel F & Dickinson MH The visual control of landing and obstacle avoidance in the fruit fly *Drosophila melanogaster*. *J. Exp. Biol* 215, 1783–1798 (2012). [PubMed: 22573757]
9. Branson K, Robie AA, Bender J, Perona P & Dickinson MH High-throughput ethomics in large groups of *Drosophila*. *Nat. Methods* 6, 451–457 (2009). [PubMed: 19412169]
10. Kim LH et al. Integration of Descending Command Systems for the Generation of Context-Specific Locomotor Behaviors. *Front. Neurosci* 11, 581 (2017). [PubMed: 29093660]
11. Muijres FT, Elzinga MJ, Melis JM & Dickinson MH Flies Evade Looming Targets by Executing Rapid Visually Directed Banked Turns. *Science* (80-. ) 344, 172–177 (2014).
12. Yilmaz M & Meister M Rapid Innate Defensive Responses of Mice to Looming Visual Stimuli. *Curr. Biol* 23, 2011–2015 (2013). [PubMed: 24120636]
13. Card G & Dickinson MH Visually Mediated Motor Planning in the Escape Response of *Drosophila*. *Curr. Biol* 18, 1300–1307 (2008). [PubMed: 18760606]
14. Borst A Time course of the Houseflies' landing response. *Biol. Cybern* 54, 379–383 (1986).
15. Borst A & Bahde S What Kind of Movement Detector is Triggering the Landing Response of the Housefly? *Biol. Cybern* 55, 65–69 (1986).
16. Bacon JP & Strausfeld NJ The dipteran 'Giant fibre' pathway: neurons and signals. *J. Comp. Physiol. A* 158, 529–548 (1986).
17. Namiki S, Dickinson MH, Wong AM, Korff W & Card GM The functional organization of descending sensory-motor pathways in *drosophila*. *Elife* 7, (2018).
18. Goodman LJ The Landing Responses of Insects. *J. Exp. Biol* 37, (1960).
19. Baines RA, Uhler JP, Thompson A, Sweeney ST & Bate M Altered electrical properties in *Drosophila* neurons developing without synaptic transmission. *J. Neurosci* 21, 1523–31 (2001). [PubMed: 11222642]
20. Borst A & Bahde S Visual information processing in the fly's landing system. *J. Comp. Physiol. A* 163, 167–173 (1988).
21. May ML & Hoy RR Leg-induced steering in flying crickets. *J. Exp. Biol* 151, 485–488 (1990).
22. Nolen TG & Hoy RR Initiation of behavior by single neurons: the role of behavioral context. *Science* 226, 992–4 (1984). [PubMed: 6505681]
23. Huston SJ & Krapp HG Nonlinear Integration of Visual and Haltere Inputs in Fly Neck Motor Neurons. *J. Neurosci* 29, 13097–13105 (2009). [PubMed: 19846697]

24. Bacon JP, Thompson KS & Stern M Identified octopaminergic neurons provide an arousal mechanism in the locust brain. *J. Neurophysiol* 74, 2739–2743 (1995). [PubMed: 8747228]
25. Suver MP, Mamiya A & Dickinson MH Octopamine neurons mediate flight-induced modulation of visual processing in drosophila. *Curr. Biol* 22, 2294–2302 (2012). [PubMed: 23142045]
26. Tuthill JC, Nern A, Rubin GM & Reiser MB Wide-Field Feedback Neurons Dynamically Tune Early Visual Processing. *Neuron* 82, 887–895 (2014). [PubMed: 24853944]
27. Riemensperger T et al. Behavioral consequences of dopamine deficiency in the *Drosophila* central nervous system. *Proc. Natl. Acad. Sci. U. S. A* 108, 834–9 (2011). [PubMed: 21187381]
28. Mamiya A, Straw AD, Tomasson E & Dickinson MH Active and Passive Antennal Movements during Visually Guided Steering in Flying *Drosophila*. *J. Neurosci* 31, 6900–6914 (2011). [PubMed: 21543620]
29. Ramirez JM Interneurons in the suboesophageal ganglion of the locust associated with flight initiation. *J. Comp. Physiol. A* 162, 669–685 (1988).
30. Maimon G Modulation of visual physiology by behavioral state in monkeys, mice, and flies. *Curr. Opin. Neurobiol* 21, 559–564 (2011). [PubMed: 21628097]
31. Suver MP, Huda A, Iwasaki N, Safarik S & Dickinson MH An Array of Descending Visual Interneurons Encoding Self-Motion in *Drosophila*. *J. Neurosci* 36, 11768–11780 (2016). [PubMed: 27852783]
32. Zorovic M & Hedwig B Processing of species-specific auditory patterns in the cricket brain by ascending, local, and descending neurons during standing and walking. *J. Neurophysiol* 105, 2181–2194 (2011). [PubMed: 21346206]
33. Hoy R, Nolen T & Brodfuehrer P The neuroethology of acoustic startle and escape in flying insects. *J. Exp. Biol* 146, 287–306 (1989). [PubMed: 2689567]
34. Staudacher E, Schildberger K Gating of sensory responses of descending brain neurones during walking in crickets. *J. Exp. Biol* 201 (Pt 4), 559–72 (1998). [PubMed: 9438831]
35. Haag J, Wertz A & Borst A Central gating of fly optomotor response. *Proc. Natl. Acad. Sci. U. S. A* 107, 20104–9 (2010). [PubMed: 21045125]
36. Kozlov AK, Kardamakis AA, Hellgren Kotaleski J & Grillner S Gating of steering signals through phasic modulation of reticulospinal neurons during locomotion. *Proc. Natl. Acad. Sci* 111, 3591–3596 (2014). [PubMed: 24550483]
37. Grillner S, Hellgren J, Ménard A, Saitoh K & Wikström MA Mechanisms for selection of basic motor programs - Roles for the striatum and pallidum. *Trends in Neurosciences* 28, 364–370 (2005). [PubMed: 15935487]
38. Maimon G, Straw AD & Dickinson MH Active flight increases the gain of visual motion processing in *Drosophila*. *Nat. Neurosci* 13, 393–399 (2010). [PubMed: 20154683]
39. Suver MP, Mamiya A & Dickinson MH Octopamine neurons mediate flight-induced modulation of visual processing in drosophila. *Curr. Biol* 22, 2294–2302 (2012). [PubMed: 23142045]
40. Chiappe ME, Seelig JD, Reiser MB & Jayaraman V Walking modulates speed sensitivity in drosophila motion vision. *Curr. Biol* 20, 1470–1475 (2010). [PubMed: 20655222]
41. Coen P, Xie M, Clemens J & Murthy M Sensorimotor Transformations Underlying Variability in Song Intensity during *Drosophila* Courtship. *Neuron* 89, 629–644 (2016). [PubMed: 26844835]
42. Ribeiro IMA et al. Visual Projection Neurons Mediating Directed Courtship in *Drosophila*. *Cell* 174, 607–621.e18 (2018). [PubMed: 30033367]
43. Fotowat H, Fayyazuddin A, Bellen HJ & Gabbiani F A novel neuronal pathway for visually guided escape in *Drosophila melanogaster*. *J. Neurophysiol* 102, 875–85 (2009). [PubMed: 19474177]
44. Sanes JR & Zipursky SL Design Principles of Insect and Vertebrate Visual Systems. *Neuron* 66, 15–36 (2010). [PubMed: 20399726]
45. Tovote P et al. Midbrain circuits for defensive behaviour. *Nature* 534, 206–212 (2016). [PubMed: 27279213]

## Methods-only References

46. Pfeiffer BD, Truman JW & Rubin GM Using translational enhancers to increase transgene expression in *Drosophila*. *Proc. Natl. Acad. Sci* 109, 6626–6631 (2012). [PubMed: 22493255]
47. Klapoetke NC et al. Independent optical excitation of distinct neural populations. *Nat. Methods* 11, 338–346 (2014). [PubMed: 24509633]
48. Tuthill JC, Nern A, Holtz SL, Rubin GM & Reiser MB Contributions of the 12 Neuron Classes in the Fly Lamina to Motion Vision. *Neuron* 79, 128–140 (2013). [PubMed: 23849200]
49. Pfeiffer BD, Ngo TTB, Hibbard KL, Murphy C, Jenett A, Truman JW, and Rubin GM (2010). Refinement of tools for targeted gene expression in *Drosophila*. *Genetics* 186, 735–755. [PubMed: 20697123]
50. Nern A, Pfeiffer BD & Rubin GM Optimized tools for multicolor stochastic labeling reveal diverse stereotyped cell arrangements in the fly visual system. *Proc. Natl. Acad. Sci* 112, E2967–E2976 (2015). [PubMed: 25964354]
51. Gouwens NW & Wilson RI Signal Propagation in *Drosophila* Central Neurons. *J. Neurosci* 29, 6239–6249 (2009). [PubMed: 19439602]
52. Lindsay T, Sustar A & Dickinson M The Function and Organization of the Motor System Controlling Flight Maneuvers in Flies. *Curr. Biol* 27, 345–358 (2017). [PubMed: 28132816]
53. Reiser MB & Dickinson MH A modular display system for insect behavioral neuroscience. *J. Neurosci. Methods* 167, 127–139 (2008). [PubMed: 17854905]
54. Williamson WR, Peek MY, Breads P, Coop B & Card GM Tools for Rapid High-Resolution Behavioral Phenotyping of Automatically Isolated *Drosophila*. *Cell Rep* 25, 1636–1649.e5 (2018). [PubMed: 30404015]
55. Brainard DH The Psychophysics Toolbox. *Spat. Vis* 10, 433–436 (1997). [PubMed: 9176952]
56. Gabbiani F, Krapp HG & Laurent G Computation of object approach by a wide-field, motion-sensitive neuron. *J. Neurosci* 19, 1122–1141 (1999). [PubMed: 9920674]
57. Iain O A Multifunctional Role for Octopamine in Locust Flight. *Annu. Rev. Entomol* 38, 227–250 (1993).
58. Burgos-Artizzu XP, Perona P & Dollar P Robust face landmark estimation under occlusion. in *Proceedings of the IEEE International Conference on Computer Vision* 1513–1520 (2013). doi:10.1109/ICCV.2013.191
59. Ozuyisal M, Calonder M, Lepetit V & Fua P Fast Keypoint Recognition Using Random Ferns. *IEEE Trans. Pattern Anal. Mach. Intell* 32, 448–61 (2010). [PubMed: 20075471]

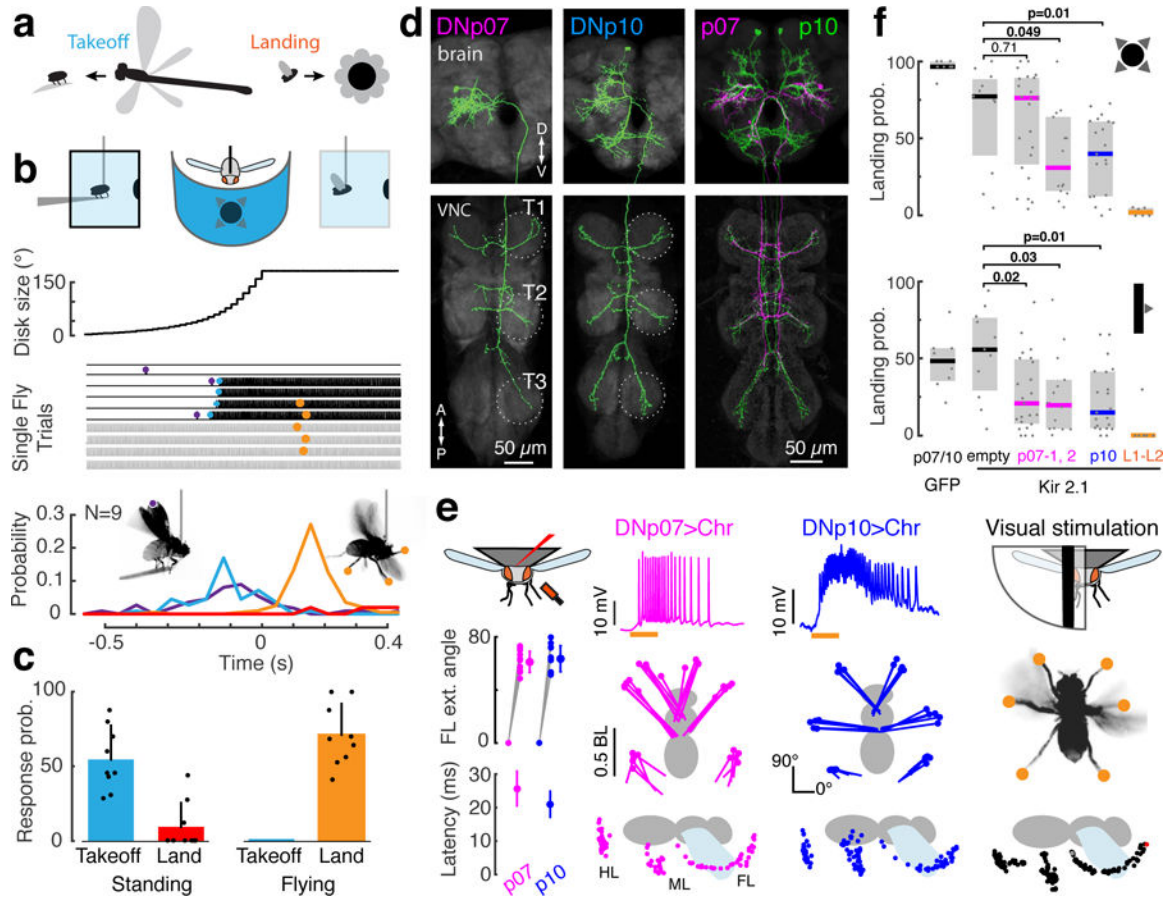


**Fig. 1. Two identified DN types contribute to visually-evoked landing responses in *Drosophila***  
**(a)** Visual looming patterns on the fly's eye can derive from different sources, including predation or self-motion towards objects. **(b)** Behavioral responses of tethered flies to a looming disk stimulus ( $r/v = 80$  ms) displayed in the frontal visual field. For single trials, vertical dashes indicate wing beats; purple, start of wing-raising; blue, flight start; orange, landing response; red line, landing probability in non-flight bouts. **(c)** Takeoff or landing probability given the fly's behavioral state (perching or flying). Dots, individuals; bars, mean  $\pm$  SD;  $n = 25$  trials each from  $N = 9$  flies. **(d)** Aligned confocal images of DNp07 and DNp10 anatomy. T1–3: segmental thoracic ganglia. Similar results were obtained from  $N = 4$  flies per DN. **(e)** Optogenetic activation of DNp07 or DNp10 drove landing responses in flying flies. Left column: mean  $\pm$  SD front leg extension angle (top,  $n = 12$  front legs from  $N = 6$  flies), and movement latency after LED on (bottom,  $n = 21$  trials,  $N = 7$  flies). Middle columns: DN membrane potential (top; orange, 50 ms LED on), and ventral (middle) or sagittal (bottom) views. Dots, leg tips at peak extension (middle,  $N = 1$  fly,  $n = 5$  trials) or every 5 ms (bottom; single trial). The LED was on for 300 ms (ventral views) or 50 ms (sagittal views). BL, body length; FL/ML/HL, front/middle/hind leg. Right column, Leg extension in response to unilateral expansion stimuli ( $10^\circ$  wide bar,  $1000^\circ/s$  front-to-back; see also Supplementary Figure 4). **(f)** Landing response probability (median  $\pm$  IQR; dots, individual flies) for frontal looming (top,  $r/v = 80$  ms) and unilateral expansion (bottom,  $500^\circ/s$  front-to-back moving bars) after silencing by Kir2.1 channel expression (p07: left,

DNp07-split-GAL4–2, right, DNp07-split-GAL4–1; for other genotypes see Methods); Two-sided Wilcoxon rank sum test.  $N_{\text{GFP}} = 8$  flies;  $N_{\text{empty}} = 11$ ;  $N_{\text{p07}_2} = 23$ ;  $N_{\text{p07}_1} = 14$ ,  $N_{\text{p10}} = 21$ ;  $N_{\text{L1-L2}} = 6$ .

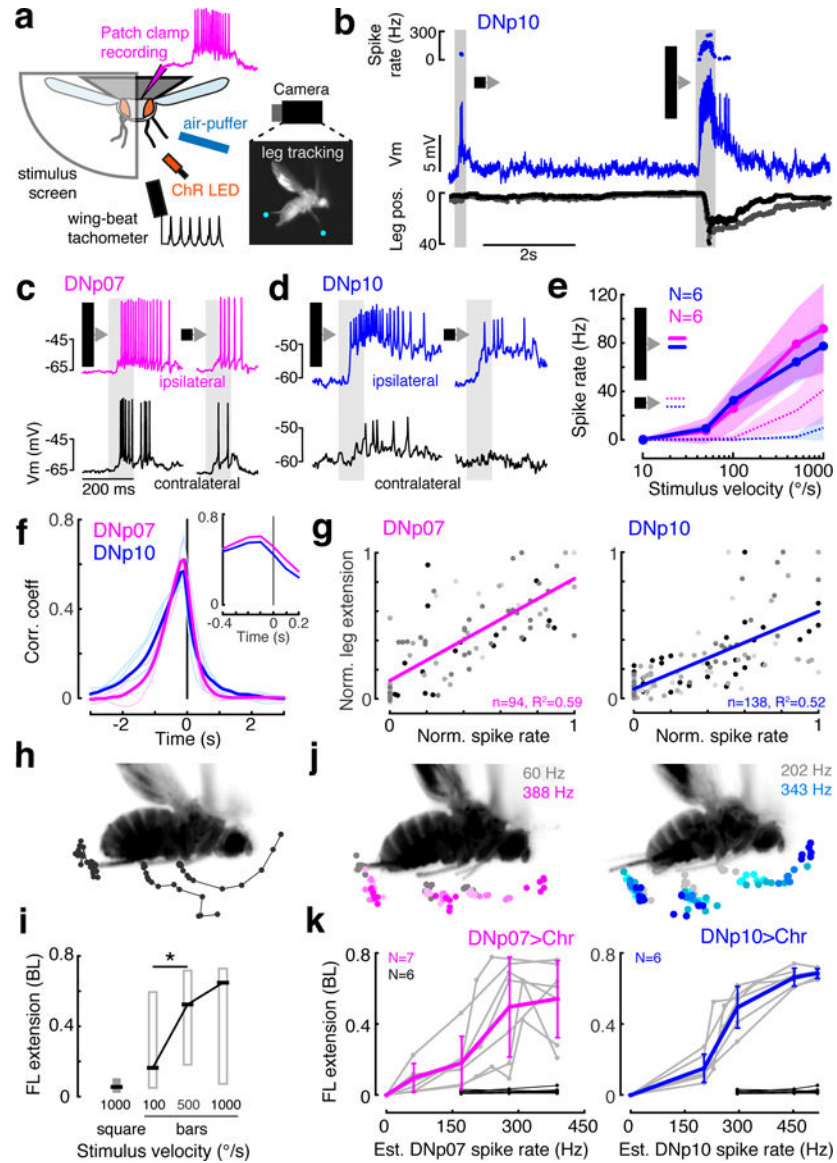


**Fig. 2. Landing DNs respond to visual stimuli and control leg extension amplitude.** (a) *in vivo* fly patch-clamp electrophysiology setup. (b) Example DNp10 recording with simultaneous leg tracking; top, instantaneous spike rate; middle: DNp10 membrane potential; bottom, horizontal deviation of each middle leg. (c–d) DNp07 (c) and DNp10 (d) activity during  $10^\circ$ -wide bar (left) or  $10^\circ \times 10^\circ$  square (right) stimulus moving front-to-back at  $1000^\circ/\text{s}$ . (e) Mean  $\pm$  SD DN responses to ipsilateral front-to-back motion of bars (solid lines) and small squares (dashed lines). (f) Cross-correlation of spike rate and middle leg movement (see Supplementary Figure 6c). Thin lines, individuals; thick lines, means for  $N = 4$  flies. The average cross-correlation peaked at  $-100$  ms in both DNs (inset). (g) Correlation of normalized mean DN spike rates with peak leg extension amplitude for individual trials. Gray levels, different flies; lines, linear fits. (h) Example leg movement response to  $1000^\circ/\text{s}$  bar; dots, leg tip positions every 5 ms until peak. (i) Box plots (median  $\pm$  IQR) of leg extension amplitude in response to front-to-back motion ( $^\circ/\text{s}$ ),  $*p=0.038$  (two-sided

Wilcoxon rank sum test),  $n_{\text{square}} = 21$ ,  $n_{\text{bar100}} = 38$ ,  $n_{\text{bar500}} = 39$ ,  $n_{\text{bar1000}} = 38$  trials,  $N = 5$  flies. **(j)** Peak ipsilateral leg tip positions. Color, estimated optogenetically-activated DN spike rate (see Supplementary Figure 7); single fly example. **(k)** Peak leg extension as a function of estimated activated DN spike rate. Gray, individuals; colored, mean  $\pm$  SD. Black, empty-split-GAL4>UAS-CsChrimson control flies. Note, these are plotted for the three highest light intensities/est. spike rates, though they are not expected to exhibit DNp07 or DNp10 spikes. n, number of trials; N, number of flies.

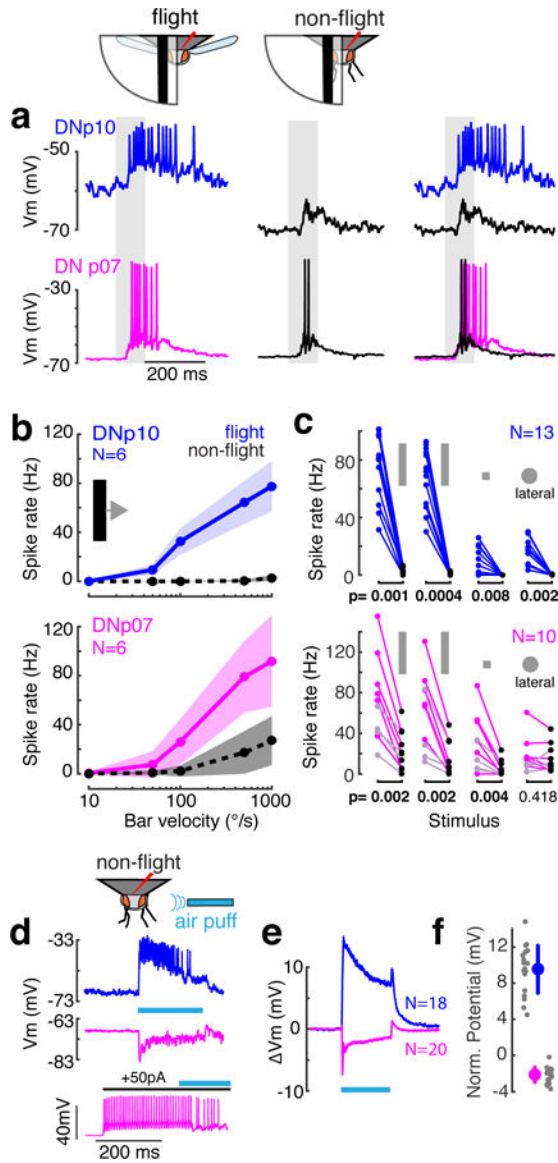


**Fig. 3: Visual responses of landing DNs are gated by flight.**

(a) Example DNp10 and DNp07 responses to ipsilateral front-to-back bar motion ( $1000^{\circ}/s$ , gray shading) during flight (colors) and non-flight bouts (black); Vm, membrane potential. Right column, overlay. (b) Mean  $\pm$  SD DN responses to bars with different velocities. (c) Individual mean DN response to visual stimuli in flight (colored dots) and non-flight (black dots) bouts. Stimuli (left to right) were  $1000^{\circ}/s$  bar,  $500^{\circ}/s$  bar,  $1000^{\circ}/s$  square, all moving front-to-back, and a lateral loom with  $r/v = 10$  (azimuth  $45^{\circ}$ , elevation  $45^{\circ}$ ). DNp07 light-colored dots, contralateral recordings, all others ipsilateral; p-values, two-sided Wilcoxon-Signed Rank test. (d) Example DN responses to mechanosensory stimulation by air puffs (cyan line). DNp10 (top) was excited, whereas DNp07 (middle) was inhibited strongly enough to inhibit spiking (bottom). All data in d-f from non-flying flies. (e) Mean DN membrane potential during air puff stimulation. (f) Individual (gray) and grand means  $\pm$  SD

(large dots) of membrane potential during last 900 ms of air puff. Sample sizes as in e. N, number of recordings from different flies

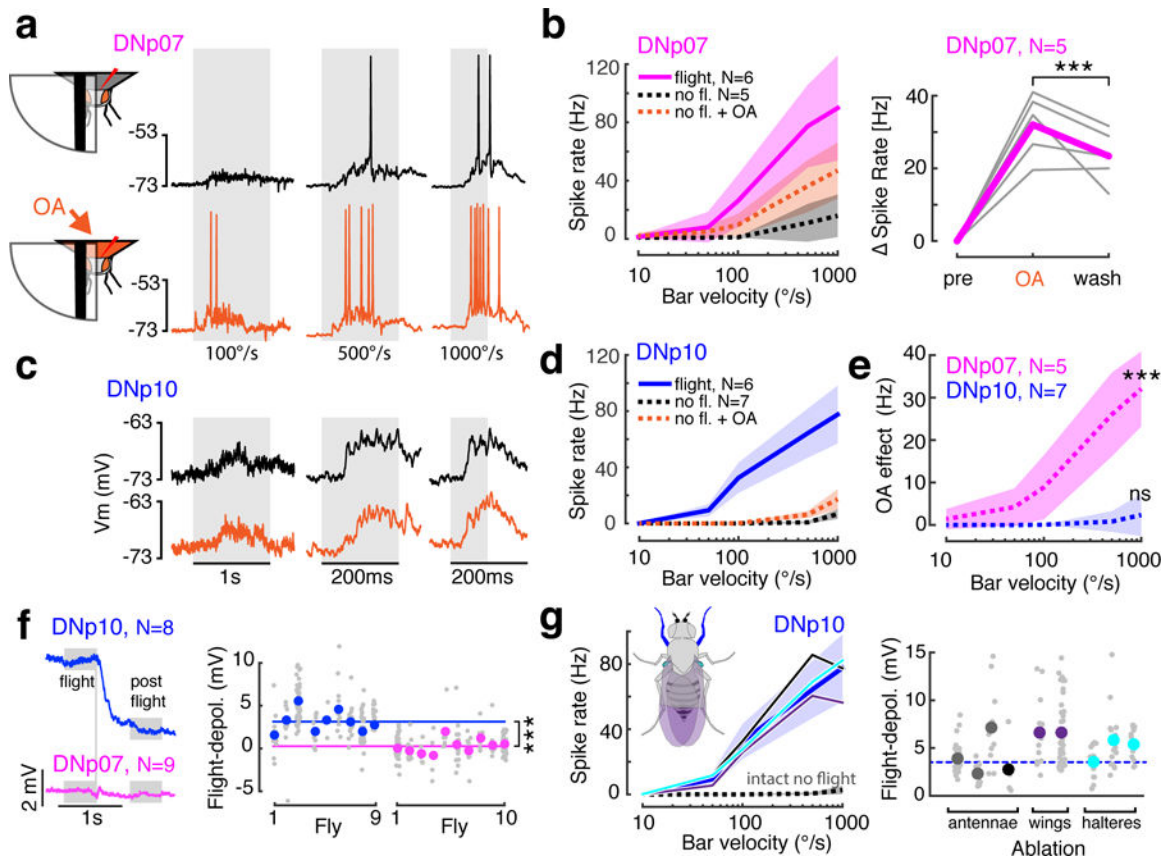


**Fig. 4: Decoupling of visual and motor circuits is achieved by different mechanisms in the two landing DN types.**

(a) Example DNp07 responses to front-to-back moving bars in non-flying flies before (black) or during (orange) brain perfusion with octopamine (OA). Gray shading, stimuli. (b) Left, mean  $\pm$  SD DNp07 responses to moving front-to-back bars of different speeds during flight, non-flight, and non-flight with OA conditions. Right, DNp07 change in spike rate compared to pre-OA condition for responses to 1000°/s front-to-back moving bar under OA and post-OA washout conditions, \*\*\* $p = 0.0014$ , paired two-sided Wilcoxon signed rank test,  $n = 34$  trials/condition). Gray, individual means; magenta, grand mean. (c–d) Example DNp10 before and during OA application (plot details as in a–b). (e) Quantification of OA effect in non-flying flies (mean  $\pm$  SD across  $N$  flies), calculated as mean response with OA minus response before OA. \*\*\*,  $p = 7.63 \times 10^{-10}$ , two-sided Wilcoxon rank sum test,  $n = 29$  trials before, and  $n = 44$  trials during OA application. n.s.,  $p = 0.24$ , two-sided Wilcoxon rank sum test,  $n = 45$  trials before, and  $n = 71$  trials during OA application. (f) DNp07 and DNp10 mean baseline membrane potential aligned by time flight stopped spontaneously (vertical gray line). Right, per-fly membrane potential difference during flight and post-flight states (gray boxes). Gray dots, trials; colored dots, single fly mean; colored lines, mean across flies. DNp10 across fly mean, 3.33 mV,  $n = 222$  trials; DNp07, 0.22 mV,  $n = 215$  trials; this difference was significant, two-sided t-test, \*\*\* $p = 3 \times 10^{-57}$ ,  $t = -18.6$ ,  $df = 435$ . (g) DNp10 visual responses (left) and the flight-dependent depolarization (right) after ablation of appendages with mechanoreceptors: antennae (single antenna, gray, both antennae, black), wings (purple), halteres (cyan); dark blue line and shaded area, response

mean  $\pm$  SD of intact flies. left:  $N_{\text{intact}} = 6$ ,  $N_{\text{antennae}} = 2$ ,  $N_{\text{wings}} = 2$ ,  $N_{\text{halteres}} = 3$ ; right:  $N_{\text{antennae}} = 4$ ,  $N_{\text{wings}} = 2$ ,  $N_{\text{halteres}} = 3$ . N, number of recordings from different flies.